Titan's winter polar vortex structure revealed by chemical tracers

Nicholas A. Teanby, Remco de Kok, Patrick G. J. Irwin, S. Osprey, Sandrine Vinatier, Peter J. Gierasch, Peter L. Read, Michael Flasar, Barney J. Conrath, Richard K. Achterberg, et al.

Titan's winter polar vortex structure revealed by chemical tracers

N. A. Teanby,[1] R. de Kok,[1] P. G. J. Irwin,[1] S. Osprey,[1] S. Vinatier,[2] P. J. Gierasch,[3] P. L. Read,[1] F. M. Flasar,[4] B. J. Conrath,[3] R. K. Achterberg,[5] B. Bézard,[2] C. A. Nixon,[5] and S. B. Calcutt[1]

Received 11 June 2008; revised 21 August 2008; accepted 15 September 2008; published 2 December 2008.

[1] The winter polar vortex on Saturn's largest moon Titan has profound effects on atmospheric circulation and chemistry and for the current northern midwinter season is the major dynamical feature of Titan's stratosphere and mesosphere. We use 2 years of observations from Cassini's composite infrared spectrometer to determine cross sections of five independent chemical tracers (HCN, HC_3N, C_2H_2, C_3H_4, and C_4H_2), which are then used to probe dynamical processes occurring within the vortex. Our results provide compelling evidence that the vortex acts as a strong mixing barrier in the stratosphere and mesosphere, effectively separating a tracer-enriched air mass in the north from air at lower latitudes. In the mesosphere, above the level of the vortex jet, a tracer-depleted zone extends away from the north pole toward the equator and enrichment is confined to high northern latitudes. However, below this level, mixing processes cause tongues of gas to extend away from the polar region toward the equator. These features are not reproduced by current general circulation models and suggest that a residual polar circulation is present and that waves and instabilities form a more important part of Titan's atmospheric dynamics than previously thought. We also observe an unexpected enrichment of C_4H_2 in the northern stratosphere, which suggests photochemical polymerization of C_2H_2. Our observations provide stringent new constraints for dynamical and photochemical models and identify key polar processes for the first time. Some of the processes we see have analogues in Earth's polar vortex, while others are unique to Titan.

Citation: Teanby, N. A., et al. (2008), Titan's winter polar vortex structure revealed by chemical tracers, *J. Geophys. Res.*, *113*, E12003, doi:10.1029/2008JE003218.

1. Introduction

[2] Titan is unique in the solar system because it has a thick atmosphere dominated by nitrogen and methane with an active photochemical cycle. Understanding processes occurring within Titan's atmosphere is a major goal of the Cassini-Huygens mission, which arrived at the Saturnian system in July 2004 and has been returning data ever since. Titan lies in Saturn's equatorial plane and takes 15.9 Earth days to complete one orbit. Rotation of Titan is tidally locked so that the same face is always toward Saturn, resulting in a day that is the same length as the orbital period. Titan experiences seasons because of Saturn's obliquity of 26.7° and has a year lasting 29.5 Earth years. Titan is currently experiencing northern midwinter and so far the Cassini data set covers early to mid northern winter. For the current season atmospheric temperature cross sections obtained by Cassini's Composite Infrared Spectrometer (CIRS) [*Flasar et al.*, 2005; *Achterberg et al.*, 2008a] provide strong evidence for a polar vortex in the (northern) winter hemisphere with a circumpolar jet located at around 30–50°N and 300 km altitude, which exhibits winds of up to 190 m s^{-1}, the fastest anywhere on Titan. The vortex has profound effects on the entire atmosphere but until now major dynamical processes occurring within the vortex have remained unconstrained, resulting in discrepancies between observations and model predictions [*Crespin et al.*, 2008; *Teanby et al.*, 2008b]. CIRS has recently built up a data set large enough to determine chemical species distributions within the vortex itself. These species act as atmospheric tracers and allow us to probe never before seen aspects of the vortex structure.

[3] Photochemical reactions [*Wilson and Atreya*, 2004] in Titan's upper atmosphere (>500 km) produce a vast array of minor species, including hydrocarbon and nitrile gases, which are eventually removed by condensation in the lower stratosphere (≈100 km). This source-sink relationship creates equilibrium gas profiles with a positive concentration gradient with respect to altitude in the stratosphere (50–300 km) and mesosphere (300–500 km). As a consequence of this gradient, these species can be used as tracers of atmospheric motion. For example, currently subsidence at

[1]Atmospheric, Oceanic and Planetary Physics, University of Oxford, Oxford, UK.
[2]Observatoire de Paris, LESIA, Meudon, France.
[3]Department of Astronomy, Cornell University, Ithaca, New York, USA.
[4]NASA Goddard Space Flight Center, Greenbelt, Maryland, USA.
[5]Department of Astronomy, University of Maryland, College Park, Maryland, USA.

0148-0227/08/2008JE003218

Table 1. Summary of Cassini-CIRS Observations Used to Obtain the Atmospheric Cross Sections in Figure 3[a]

Date	Latitude (°N)	Longitude (°W)	Orbit	N	FOV Size (km)
15 Jan 2006	53.7	65.1	20	730	42
20 May 2006	−33.6	−120.9	24	260	50
20 May 2006	51.4	−99.7	24	793	43
2 Jul 2006	−53.8	−80.4	25	531	40
21 Jul 2006	46.6	−122.1	26	300	49
9 Oct 2006	61.0	−87.7	30	638	43
9 Oct 2006	29.2	41.0	30	419	40
12 Dec 2006	16.1	−111.1	35	271	48
12 Jan 2007	3.7	33.1	37	685	42
29 Jan 2007	29.6	−19.1	38	727	41
25 Mar 2007	−20.6	143.0	41	715	44
30 Aug 2007	68.5	101.7	49	391	45
21 Dec 2007	−46.2	−74.9	54	786	45

[a]N is the number of spectra used from each observation. FOV size is the projected diameter of the field of view on Titan's limb.

the northern winter pole brings tracer-enriched air from the upper atmosphere into the lower atmosphere where it can be observed and used as a diagnostic for atmospheric circulation [*Teanby et al.*, 2008a]. Titan's minor species have a large range of lifetimes, from a few weeks to several thousand years, which means that they are sensitive to atmospheric dynamics over a range of timescales and different gases can be used to study different aspects of the vortex. Cassini-CIRS is uniquely able to measure Titan's trace gas abundances with sufficient spatial resolution to allow indirect imaging of chemical and dynamical processes occurring within the vortex.

[4] The behavior of Titan's meridional stratospheric and mesospheric circulation can be split into three main seasonal regimes. Around the equinoxes, models predict a transitional regime of two symmetrical meridional cells, comprising rising air at the equator and subsiding air at the poles [*Hourdin et al.*, 1995; *Tokano et al.*, 1999; *Hourdin et al.*, 2004; *Rannou et al.*, 2005; *Richardson et al.*, 2007]. During interequinox periods this pattern quickly becomes unstable and is replaced by a single south-north (north-south) cell during northern winter (summer).

[5] These predictions are in broad agreement with observations of trace gas enrichment at northern latitudes determined previously with Cassini-CIRS nadir (downward looking) data [*Flasar et al.*, 2005; *Teanby et al.*, 2006; *Coustenis et al.*, 2007; *Teanby et al.*, 2008a, 2008b]. These observations suggest that circulation in Titan's stratosphere/mesosphere currently comprises a single meridional circulation cell with an upper branch flowing from the summer (south) to winter (north) pole. However, these nadir studies were generally only sensitive to a single atmospheric level and provide very limited information on vertical atmospheric structure. The best way of determining detailed horizontal and vertical atmospheric structure is by observing spectra in a limb viewing geometry (toward the horizon) at multiple latitudes. A recent study has used such observations to obtain a cross section of the vortex zonal mean temperature structure [*Achterberg et al.*, 2008a], which can be used to derive zonal mean thermal winds, defining the vortex jet structure. However, to constrain transport and chemical processes occurring within the vortex composition profiles are also required. So far, composition studies using limb data [*Teanby et al.*, 2007; *Vinatier et al.*, 2007; *Vinatier*, 2007] have only probed a few discrete latitudes or have been at very low spectral resolution with large uncertainties. While these studies give important information on vertical abundances, they do not provide a complete picture of vortex structural composition, which is essential for understanding Titan's complex polar interactions and for advancing numerical models to the next level.

[6] In this paper we use Cassini-CIRS limb spectra to determine altitude-latitude cross sections of vortex composition during Titan's midwinter season (2006 and 2007).

2. CIRS Data

[7] CIRS is a Fourier transform spectrometer that records spectra in the far- and mid-IR (10–1500 cm^{-1}, 1 mm to 7 μm). This spectral range covers emission features of most of Titan's photochemical inventory and spectra can be used to derive atmospheric temperature and composition. The full spectral range of CIRS is covered by three separate focal planes, which use the same telescope and scan mechanism: FP1 10–600 cm^{-1} (far-IR); FP3 600–1100 cm^{-1} (mid-IR); and FP4 1100–1500 cm^{-1} (mid-IR).

[8] The apodized spectral resolution of CIRS is adjustable between 0.5 and 15.5 cm^{-1}. Here, we use high (0.5 cm^{-1}) spectral resolution mid-IR data from FP3 and FP4 as this allows unambiguous identification of spectral emission features from Titan's diverse range of constituent gases. In limb-viewing geometry these spectral regions are most sensitive to temperature and composition of the stratosphere and lower mesosphere (150–500 km).

[9] FP3 and FP4 each comprise a linear array of 10 square pixels with a small field of view (0.27 × 0.27 mrad), which allows limb measurements of Titan's atmosphere to determine temperature and composition with vertical resolutions of less than an atmospheric scale height (20–40 km). More detailed information on CIRS can be found in *Kunde et al.* [1996] and *Flasar et al.* [2004].

[10] In total we used 13 observation sequences from 11 Titan flybys taken from January 2006 to December 2007 (Table 1). Each observation sequence was acquired in a limb staring mode, in which the linear pixel arrays were aligned perpendicular to Titan's horizon and limb spectra were repeatedly measured at the same location. This type of observation typically had a duration of around 4 h and was taken when Cassini was approximately 150,000 km from Titan. To increase the signal-to-noise ratio, the multiply observed altitude-radiance profiles were averaged together by fitting a smooth spline function [*Teanby*, 2007] with a knot spacing of 30 km to the measured radiances at each wave number as in the work by *Teanby et al.* [2007].

[11] Typically, during each Titan flyby, time constraints meant that only one or two latitudes and longitudes could be observed in this configuration. Therefore, to probe the vortex structure we must slowly build up a composite atmospheric cross section from multiple flybys covering the full 2 year period. This procedure assumes that (1) the atmosphere is zonally symmetric, with no longitudinal variation and (2) the large-scale atmospheric structure has not changed significantly during the 2 year observation period. While this seems like a large interpretive jump, it must be remembered that Titan's year lasts around 30 Earth years so seasonal effects are slow and numerical models

predict little change in composition during this time [*Rannou et al.*, 2005], with any temporal changes being small compared to the latitude-altitude variations considered here.

[12] In addition, these assumptions are backed up by observational evidence as follows: (1) Temperature and composition mapping by *Flasar et al.* [2005] and *Teanby et al.* [2006, 2008b] show a zonally symmetric structure, with no significant longitudinal variations. (2) Observed temporal variations in composition from the 4 years of Cassini's prime mission (2004–2008) show that since early 2006 atmospheric composition in the southern hemisphere has remained stable [*Teanby et al.*, 2008a]. We have thus restricted our analysis to data taken in 2006–2007. Slightly more variability is expected in the north but the configuration of Cassini's orbit meant that much less data are available at high northern latitudes. Therefore, it is not possible to determine reliable temporal trends in the north at present because the time series of nadir observations is very short compared to Titan's seasonal cycle [*Teanby et al.*, 2008a]. Assumption 2 is tested further in section 4.1.

3. Methods

[13] Inversion for temperature and composition from CIRS spectra is described in detail by *Teanby et al.* [2007]. In brief, we used a constrained iterative nonlinear retrieval method [*Rodgers*, 1976; *Houghton et al.*, 1984] based on the correlated-*k* approximation [*Lacis and Oinas*, 1991] as implemented by *Irwin et al.* [2008]. First, the ν_4 band of methane from 1240 to 1360 cm^{-1} (FP4) was used to determine a temperature profile for each observation assuming a stratospheric methane abundance of 1.41% as measured by the Huygens probe mass spectrometer [*Niemann et al.*, 2005]. During this stage the tangent altitude of the observation was corrected to allow for instrument pointing errors, which were typically less than 10–20 km. Second, the temperature profile was fixed and continuous profiles of the constituent gases were determined by fitting 620–733 cm^{-1} (FP3). Damping was applied to the inversion to suppress spurious unresolved vertical structure smaller than an atmospheric scale height. Additional forward modeling error was added to the measured spectra to account for small differences introduced by the correlated-*k* approximation. The altitude scale of the atmospheric profiles were determined by assuming hydrostatic equilibrium and an altitude/latitude-dependent gravity: this required us to make reasonable assumptions about temperatures in the lower stratosphere and troposphere, which were unconstrained by these observations. Spectroscopic parameters were the same as from *Teanby et al.* [2007] except that we have used updated line data for HC_3N from *Jolly et al.* [2007].

[14] To ensure that spectra were modeled accurately, we have allowed for finite field-of-view size using the method of *Teanby and Irwin* [2007], so that modelled spectra at each tangent altitude comprised an average of five spectra distributed uniformly across the field of view. This is a significant improvement over the analysis of *Teanby et al.* [2007].

[15] The contribution functions (rate of change of radiance with respect to the determined parameter) saturated at altitudes below 150 km (180 km near the north pole) and no information on atmospheric composition could be extracted below these altitudes [*Teanby et al.*, 2007]. Above 300–500 km (depending on the latitude and gas species) the signal-to-noise ratio became too low to allow a reliable composition determination. An example fit to the data is shown in Figure 1.

4. Results

4.1. Atmospheric Stability

[16] To check that Titan's atmospheric composition was stable over the 2 year observation period, we compare composition profiles obtained from our data in May 2006 and December 2007 around 40°S (Figure 2). Any changes in atmospheric composition would be most obvious in short lifetime species such as HC_3N and C_4H_2. However, for all species differences are slight and to within the error bars, indicating a stable atmospheric composition in the southern hemisphere at this time. A similar comparison is not possible in the north because of strong composition gradients and lack suitable observations. However, the consistent trend from low to high abundance of all species as we move further north, despite the disordered observation times with respect to latitude (Table 1), indicates that observed features are not artifacts. Therefore, we conclude that it is valid to collapse all our results onto single latitude-altitude atmospheric cross sections, effectively providing a good representation of the zonally averaged tracer distribution within Titan's polar vortex for midwinter.

4.2. Composition Cross Sections

[17] Figure 3 shows the combined temperature and composition cross sections for 2006–2007 (northern midwinter) derived from the Cassini-CIRS limb soundings in Table 1. The plot also includes zonal mean thermal wind contours for the vortex jet derived from temperature gradients [*Achterberg et al.*, 2008a]. The composition cross sections provide a large amount of new information about the vortex structure. However, care is taken to interpret only the gross features because of the composite nature of the data set.

[18] The most striking feature is the sharp boundary in composition seen around 60°N for all five tracers, demonstrating that isolation of enriched and unenriched air masses is occurring within the vortex. Above 300 km altitude, enrichment of trace species is confined close to the pole and composition contours appear to track those of zonal wind. However, below 300 km the enrichment extends to lower latitudes. This is visible for all species studied here, especially those with the shortest lifetimes (HC_3N and C_4H_2).

[19] For all five tracer species an unexpected feature is the extended deep abundance minimum, or mesospheric depleted zone (MDZ), occurring above the vortex circumpolar jet at around 350 km and encroaching as far north as 65°N. This is a new feature and has not been predicted by numerical models. In the case of the longest lived species (HCN) the minimum is bounded by more enriched air to the south, effectively forming a depleted torus around Titan's north pole extending over 10–20° of latitude. The existence of a mesospheric depleted zone both explains and puts into context isolated observations of abundance minima in HCN, HC_3N, C_3H_4, and C_4H_2 profiles previously reported by *Teanby et al.* [2007], *Vinatier et al.* [2007], and *Vinatier* [2007]. There is no such counterpart for Earth's polar vortex, highlighting key physical differences.

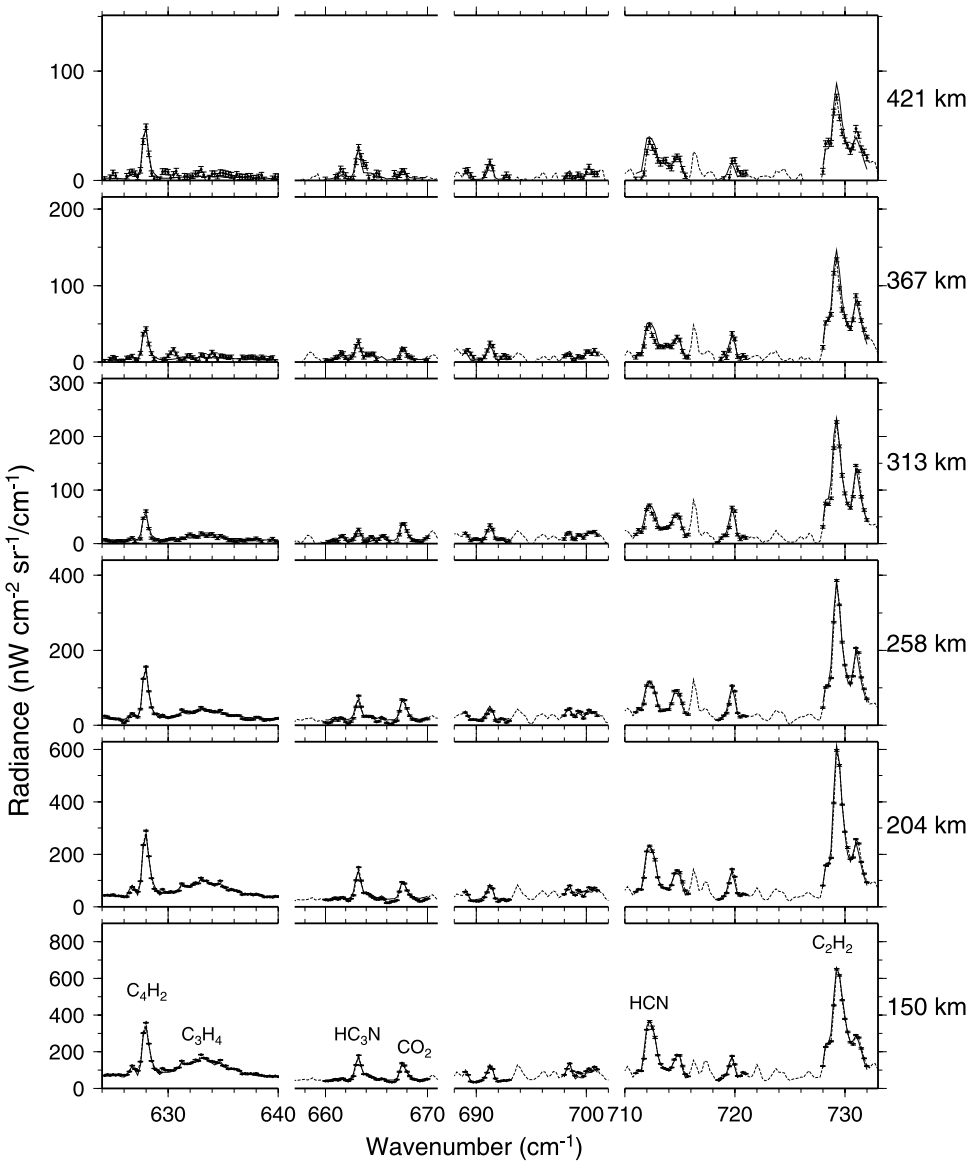

Figure 1. Example fits (solid lines) to the measured radiances (dots with error bars) at tangent altitudes from 150 to 421 km taken on 15 January 2006 at 54°N.

[20] Outside the vortex, tongues of HCN, C_2H_2, and C_4H_2 at 200–300 km altitude extend from the vortex region toward the equator, increasing in altitude toward southern latitudes. The same is not true for C_3H_4 and HC_3N.

[21] These three key observations are the main results of this paper and provide new insight into Titan's atmospheric structure.

4.3. Inversion Robustness

[22] When inverting the spectra to obtain temperature and composition profiles the two most significant undesirable effects are due to nonuniqueness and line-of-sight effects. To ensure that the observed features are robust, it is important to consider how these effects could alter the composition cross sections, especially for the mesospheric depleted zone.

4.3.1. Nonuniqueness

[23] The strength of a gas emission feature depends on both atmospheric temperature and gas abundance; so if temperature is underestimated, the abundance will be overestimated to compensate. Given limited data, there are many possible temperature structures that could fit the same observed spectra, although limb data are much less susceptible than nadir data. Our inversion process applies smoothing so that structure not resolvable by the finite field of views is suppressed in the profiles and the result is constrained to be as close as possible to an initial guess or a priori atmosphere, while still fitting the data to within the measurement errors. This is common way to address nonuniqueness in inverse problems [*Rodgers*, 1976; *Houghton et al.*, 1984]. Our a priori temperature profile is based on that obtained at 15°S by *Flasar et al.* [2005]. In the north the stratopause is much hotter than at 15°S and the lower stratosphere is much colder. Therefore, the effect of constraining the inversion is that temperatures derived for the hot northern stratopause may be slightly too cool. This can be checked by repeating the inversion using a second a priori atmosphere that is too warm; this brackets the

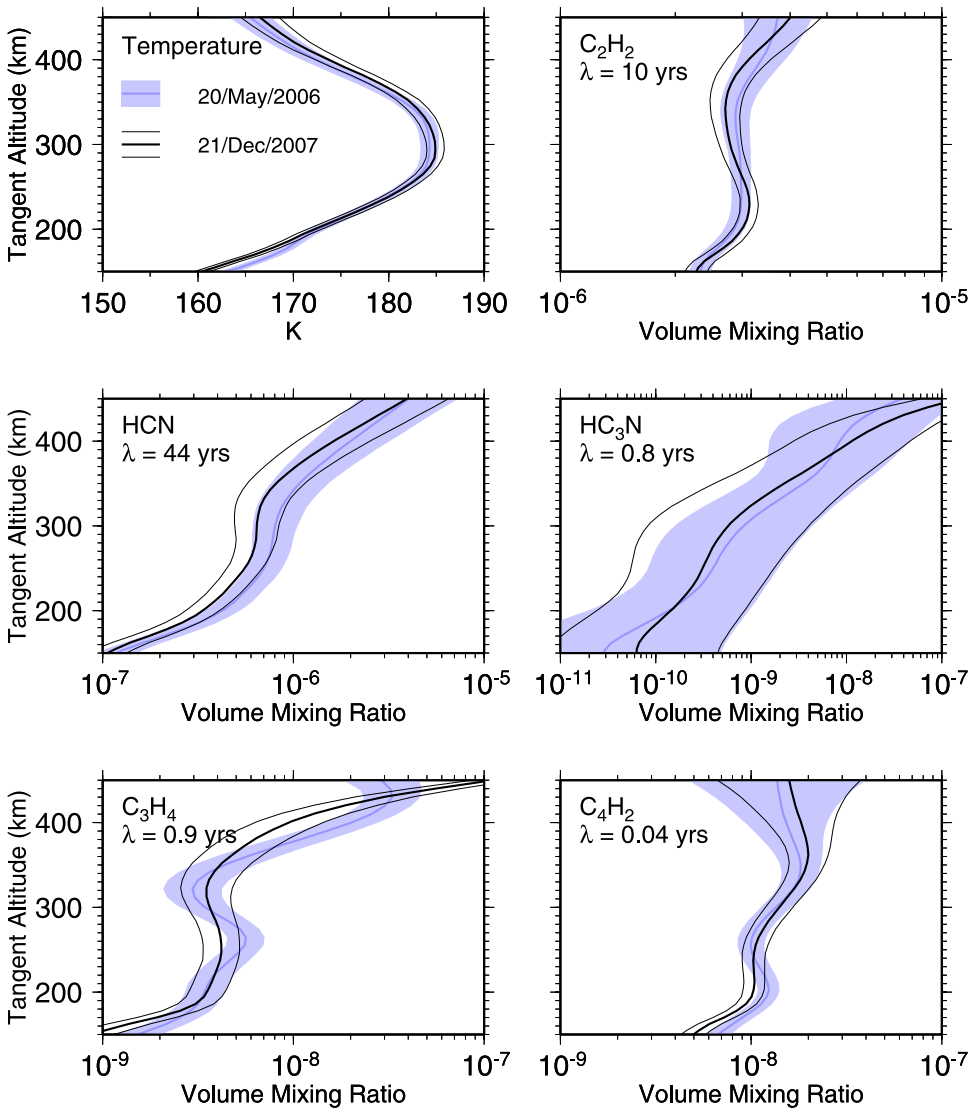

Figure 2. Comparison of composition profiles obtained at 34 and 46°S on 20 May 2006 and 21 December 2007, respectively. The profiles are consistent to within the inversion errors, showing that the southern hemisphere has a stable composition over our observation period. This allows us to confidently build an atmospheric cross section from observations taken at different times throughout 2006–2007; λ is the photochemical lifetime at 300 km from *Wilson and Atreya* [2004].

inversion and shows that differences caused by the constraints are to within the formal inversion errors. Such errors are not sufficient in size to significantly affect the composition results. In fact, because the effect of our assumed a priori is to produce temperatures that are slightly too cool at the stratopause, this would result in a slight overestimate of the abundances within the MDZ. The converse is true for the lower stratosphere. Therefore, this effect would reduce the contrast of the observed composition features slightly.

4.3.2. Line-of-Sight Effects

[24] For tangent altitudes below around 200 km the atmosphere starts to have significant opacity. This means that the effective tangent point will be closer to the spacecraft than the geometric tangent point. Therefore, when observing the north pole from an equatorial orbit a slightly lower latitude is observed than would be expected from geometry alone. This effect was studied in detail by *Achterberg et al.* [2008a], who compared 1D and 2D temperature inversion techniques. They found that assuming a 1D atmosphere structure, as we have done here, can result in underestimating the temperature by up to 4 K near the hot stratopause at high northern latitudes. In the cold lower stratosphere, the effect is to overestimate the temperature by a similar amount. This effect would not remove the composition structure we see but reduce the contrast slightly. South of 50°N this effect is not significant. A 2D inversion for composition is not possible because of the limited information contained in single gas emission peaks. Therefore, it is best to assume a 1D atmospheric structure for both temperature and composition retrievals to ensure consistency.

[25] Both nonuniqueness and line-of-sight effects would conspire to reduce the contrast of our observed composition features but could not cause their existence. Neither effect can explain the presence of a MDZ. The observed features

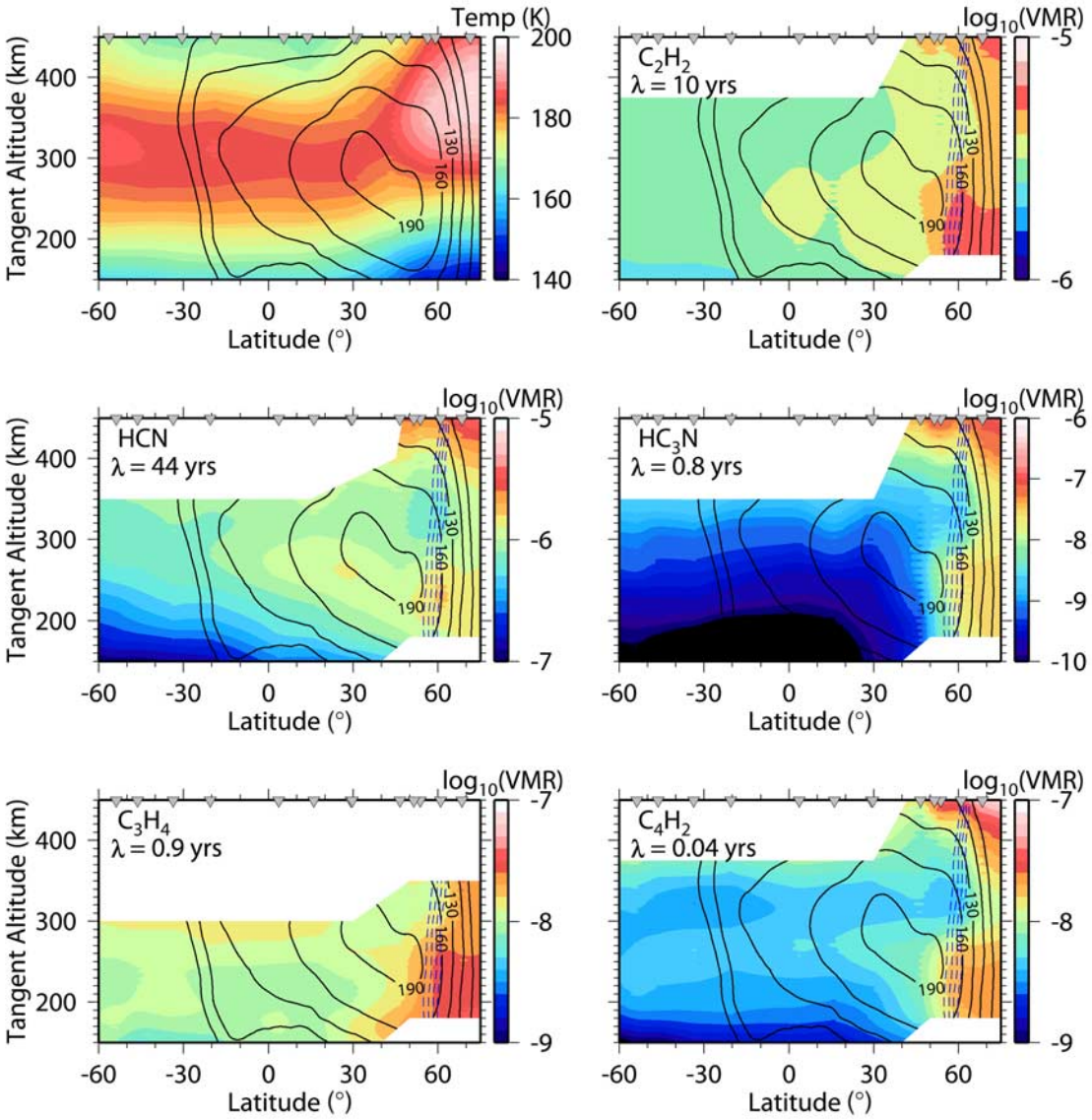

Figure 3. Cross sections of temperature and composition through Titan's atmosphere constructed using the observations in Table 1. Composition is given as a volume mixing ratio, and the positions of the observed profiles are denoted by inverted triangles at the top of each plot. Contours indicate the vortex zonal wind speeds (in m s^{-1}) derived by *Achterberg et al.* [2008a], and blue dashed lines show the region with the steepest horizontal potential vorticity gradient, which indicates a dynamical mixing barrier (see Figure 5 and section 5.1). Altitudes with low signal to noise or where the atmosphere becomes opaque are not plotted. VMR is the volume mixing ratio, and λ is the photochemical lifetime at 300 km.

are thus robust and if anything should be slightly more pronounced than in Figure 3.

5. Discussion

[26] As discussed by *Flasar et al.* [2005], *Teanby et al.* [2006, 2008a, 2008b], and *Coustenis et al.* [2007] the descending branch of the meridional circulation cell advects trace gases from their upper atmosphere source regions into the stratosphere, causing enrichment of these species in the north. This basic enrichment process provides the backdrop for our new results. In this section we develop an overall interpretation of our observations in terms of atmospheric dynamics and photochemistry, while considering important similarities between Titan and Earth's winter vortices.

[27] A schematic of our overall interpretation of processes occurring in the north polar vortex region is shown in Figure 4. The processes in this schematic are explained in detail in sections 5.1–5.5.

5.1. Isolation of Polar Air Mass

[28] The observed distributions of tracer species show that a very effective middle atmosphere mixing barrier exists at around 60°N, which isolates the enriched northern air mass from more southerly latitudes. Short lifetime species such as HC_3N display a very sharp boundary here.

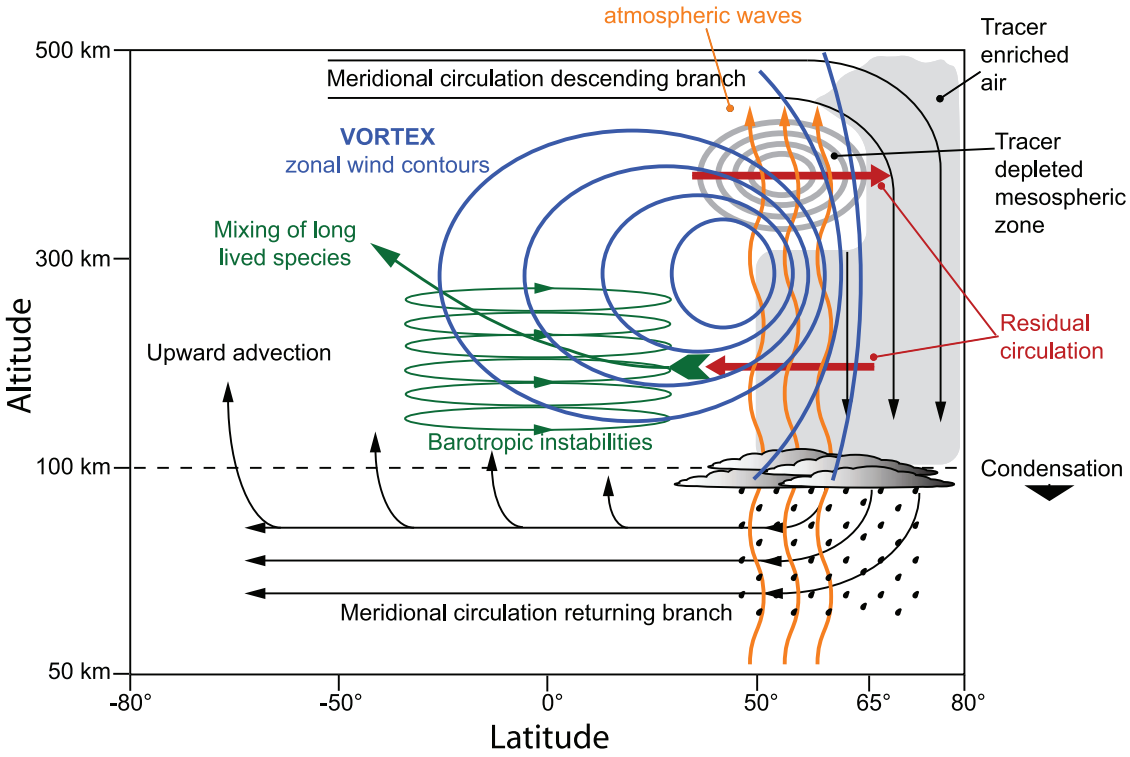

Figure 4. Schematic of the dynamical processes occurring in Titan's north polar region.

[29] We propose that this mixing barrier is a dynamical effect caused by the polar vortex. This can be investigated further by using temperature and wind fields [*Achterberg et al.*, 2008a] to determine the potential vorticity (PV).

[30] Potential vorticity is proportional to the dot product of the absolute vorticity and the gradient of potential temperature. As a consequence of Kelvin's circulation theorem, potential vorticity is conserved for adiabatic frictionless flows, so a strong horizontal gradient in PV implies horizontal mixing is inhibited, leading to an effective mixing barrier [*Andrews et al.*, 1987]. Therefore, PV effectively provides another independent tracer in addition to the composition measurements. For the Earth's polar vortex a mixing barrier is indeed associated with a steep gradient of potential vorticity [*McIntyre and Palmer*, 1983; *McIntyre*, 1989]. Following *Read et al.* [2006] potential vorticity q can be approximated by:

$$q = -g(f + \xi_\theta)\frac{\partial \theta}{\partial p} \tag{1}$$

where: g is gravitational acceleration, $f = 2\Omega\sin\phi$, Ω is the angular rotation rate of Titan, ϕ is latitude, θ is potential temperature, p is pressure, and ξ_θ is the vertical component of absolute vorticity calculated at constant potential temperature given by:

$$\xi_\theta = -\frac{1}{r^2\cos\phi}\frac{\partial}{\partial \phi}(ru\cos\phi) \tag{2}$$

We calculated the zonal velocity u using the thermal wind equation for a curved atmosphere and assuming a lower boundary condition wind velocity of 4Ω at 10 mbar [*Achterberg et al.*, 2008a] - q is then evaluated on constant θ surfaces following *Read et al.* [2006] using a finite difference technique. Because of Titan's significant atmospheric curvature the distance to Titan's center r cannot be assumed constant and must remain inside the differential term in equation (2).

[31] The potential temperature θ [*Houghton*, 2002] of a parcel of air at temperature T and pressure p is calculated by assuming the parcel is moved adiabatically to the 10 mbar pressure level:

$$\theta = T\left(\frac{p_0}{p}\right)^\kappa \tag{3}$$

where p_0 is the 10 mbar reference pressure and κ is the ratio of heat capacities $(c_p - c_v)/c_p$. Assuming a representative mean atmospheric temperature of 200 K for Titan's atmosphere and a composition of 98.6% N_2 (c_p = 29.1 J K^{-1} mol^{-1}) and 1.4% CH_4 (c_p = 33.5 J K^{-1} mol^{-1}) gives a mean specific heat capacity of c_p = 29.2 J K^{-1} mol^{-1} and a value of κ = 0.281.

[32] The $1/p$ factor causes q to increase exponentially with altitude, making horizontal trends hard to determine. *Lait* [1994] points out that scaling PV by a function θ^n preserves the relative horizontal PV gradients on surfaces of constant θ. Therefore, an appropriate choice of n can be used to remove the intrinsic exponential increase in PV with altitude, while preserving the conservative properties of PV. Lait suggests a value of $-9/2$ for an isothermal atmosphere. However, we found that the atmospheric structure of Titan is such that $-7/2$ is more effective at removing the vertical trend in PV. This makes the horizontal structure much easier to see and allows comparison of relative PV gradients at different atmospheric levels.

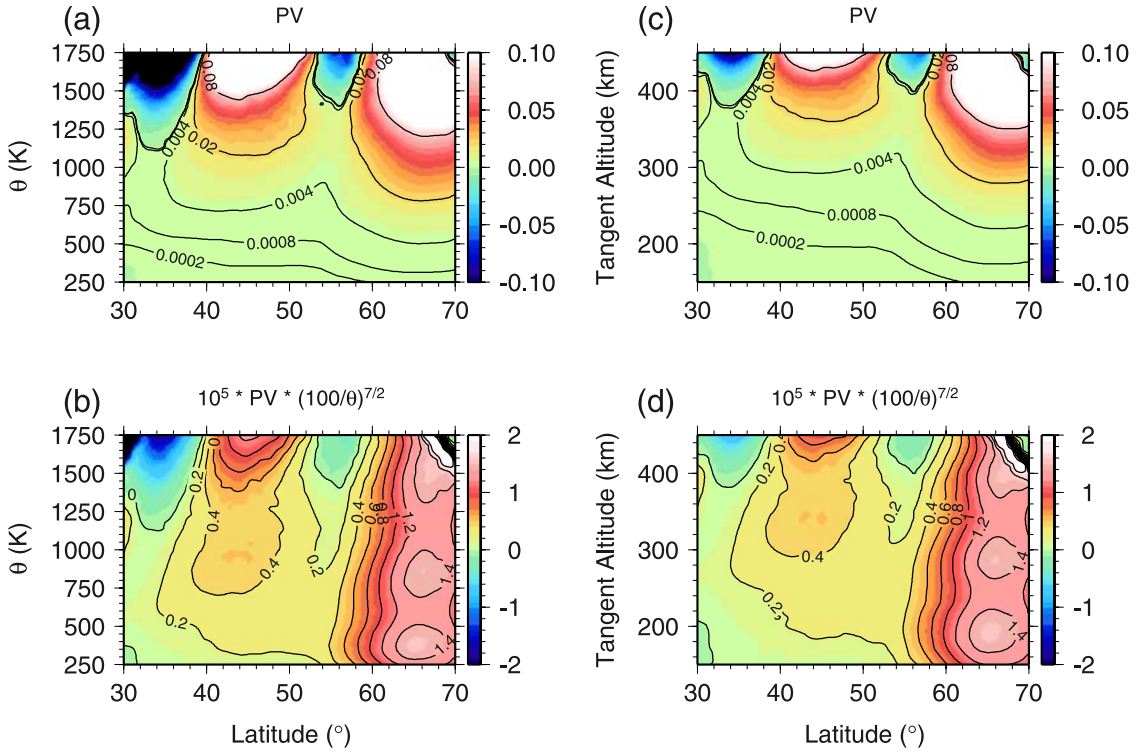

Figure 5. (a) Potential vorticity (PV) derived from the smoothed temperature cross section of *Achterberg et al.* [2008a] and assuming thermal wind balance. (b) Potential vorticity from Figure 5a modified using a scaling similar to that of *Lait* [1994] to remove the intrinsic strong altitude dependence of PV and bring out the horizontal structure. (c) and (d) Same as Figures 5a and 5b but regridded in terms of altitude. Plots cover approximately the same vertical range, but θ and altitude are not linearly related. Note that above ~400 km the determination of PV becomes susceptible to calibration effects and only gross features should be interpreted. The scaled PV (Figures 5b and 5d) shows sharp horizontal gradients at 60°N throughout the stratosphere and lower mesosphere, implying a strong dynamical resistance to horizontal mixing consistent with the observed tracer distribution.

[33] Figure 5 shows scaled and unscaled PV surfaces. Note that calculation of q effectively involves taking the second latitude derivative (curvature) of a highly smoothed temperature field and is hence susceptible to calibration subtleties at high altitudes (above 400 km). Therefore, only gross features should be interpreted. Latitudes south of 30°N are not plotted as the thermal wind equation starts to break down within 30° of the equator and at southern latitudes temperature gradients are too small to provide a reliable PV determination.

[34] The region of steepest horizontal PV gradient is indicated in Figure 3 and displays a remarkable correspondence with the mean position of the observed composition boundaries. This provides the strongest evidence to date for dynamical isolation of air inside Titan's north polar vortex and illustrates the importance of the vortex's influence on atmospheric circulation and composition in this region. Similar dynamical isolation occurs in Earth's Antarctic polar vortex, causing depletion of trace species and allowing an ozone hole to develop within the vortex [*Schoeberl and Hartmann*, 1991].

5.2. Mesospheric Depleted Zone

[35] All five tracer species show greater polar confinement at higher altitudes, which suggests a dynamical rather than a chemical origin for the mesospheric depleted zone, especially when combined with the fact that the bottom boundary of this zone occurs at a similar altitude to the vortex circumpolar jet (300 km). Evidently some secondary process is causing greater confinement at high altitude and increased equatorward transport at lower altitudes. Flat temperature contours observed in the lower stratosphere are also consistent with enhanced transport in this region. However, this could also be caused by a radiative effect due to a transition between the hot stratopause and the cold lower atmosphere, which is just exiting from an extended polar night.

[36] Equatorward transport in the stratosphere could be caused by horizontal eddies resulting from barotropic instabilities due to large horizontal wind shears close to the vortex circumpolar jet. However, the latitudinal wind gradient is such that barotropic instabilities are most likely south of the vortex jet [*Luz et al.*, 2003], whereas our observations require mixing north of the vortex jet.

[37] Our preferred interpretation is that the observed tracer distribution is caused by a residual meridional circulation near the north pole that is poleward above the vortex jet and equatorward below. The possible origin of this circulation is discussed in detail in section 5.3.

[38] Low abundances within the depleted zone could thus be a consequence of poleward advection of air from further south that has an abundance corresponding to an equilibrium

photochemical profile. This is supported by the observation that for HCN, HC_3N, and C_4H_2 abundances in the depleted zone are similar to those at southern latitudes where vertical gas profiles are close to their equilibrium conditions.

[39] The existence of a depleted zone implies that no streamlines can pass through this region from higher altitudes, otherwise enrichment would occur here because of connection with enriched air from the high-altitude photochemical production zone.

5.3. Explanation for Inferred North Polar Residual Circulation

[40] The observed mesospheric depleted zone implies that a residual circulation exists close to Titan's north pole. In this section we discuss possible origins for this inferred circulation.

[41] At Titan's south pole numerical models [e.g., *Crespin et al.* 2008] predict a residual circulation in the stratosphere extending up to the 1 mbar level, ascending at around 40°S and descending at the south pole. In the models this is driven by excess cooling at the south pole due to enriched aerosol abundances left over from southern winter/spring, which causes subsidence and acts in the opposite sense to the overall solar-heating-driven upwelling of the main meridional circulation. However, this mechanism could not explain a residual circulation at the north pole. Excess aerosol and trace gas abundances in the north would cause enhanced radiative cooling of the middle and lower stratosphere [*Bézard et al.*, 1995], but this would simply help to drive the main south-north meridional circulation cell. Also the sharp horizontal PV gradients associated with the vortex winds would inhibit such a cell.

[42] Another possibility is due to breaking atmospheric waves. Determinations of Titan's stratospheric and mesospheric winds [*Hubbard et al.*, 1993; *Achterberg et al.*, 2008a] show a superrotating atmosphere circling the moon in under 48 h, which can be explained by the Gierasch-Rossow mechanism [*Gierasch*, 1975; *Rossow and Williams*, 1979; *Hourdin et al.*, 2004]. This wind field can cause atmospheric waves to break and deposit additional momentum into the zonal flow, thus setting up a residual circulation.

[43] These waves could include gravitational tides forced by Titan's eccentric orbit [*Strobel*, 2006] or broad spectrum gravity waves generated in the lower atmosphere by convection or wind shear instabilities. Gravitational tides can have a wave number zero or two pattern, with the westward propagating wave number two component being significantly weaker than the corresponding eastward component [*Walterscheid and Schubert*, 2006]. Gravitational tides have a slower phase speed than the background flow [*Strobel*, 2006]. Therefore, they propagate westward with respect to the background flow and thus exert a drag on the background flow when they break, causing a meridional flow toward the pole. In other words, the residual meridional circulation transports angular momentum to offset the stresses from the waves and maintain a steady state. Gravitational tides have not yet been observed in Titan's stratosphere or mesosphere [*Achterberg et al.*, 2008b], although *Müller-Wodarg et al.* [2006] recently report wave structures in the thermosphere (>1000 km) that could be tidal in origin.

[44] On the other hand, gravity waves can propagate in both east and west directions with respect to the background flow and when they break can either exert an acceleration or drag on this background flow, inducing a flow either away from or toward the pole, respectively. The existence of gravity waves in Titan's atmosphere is supported by a mounting body of evidence including: the Voyager radio occultation [*Hinson and Tyler*, 1983; *Friedson*, 1994]; the Sgr28 stellar occultation [*Sicardy et al.*, 1999]; and the Huygens probe temperature profile [*Fulchignoni et al.*, 2005]. Breaking gravity waves, possibly aided by tidal waves above the vortex jet, could thus cause a poleward residual circulation in the north polar region. The occurrence of wave drag above the stratopause could help to close off the vortex jet at high altitudes, which is consistent with the observation that zonal wind speeds decrease with altitude above the stratopause at all latitudes.

[45] To investigate where gravity waves could break and how they could affect the flow, we performed a sensitivity study using the Doppler spread parameterization (DSP) of *Hines* [1997].

[46] It is assumed that most of the gravity waves seen in Titan's stratosphere originate from processes in the troposphere (e.g., convection, shear instabilities, etc.). Calculations were made determining the characteristics of momentum forcing in an idealized atmosphere characteristic of Titan. We launched a broad spectrum of waves evenly distributed about $j = 1 \ldots N_j$ azimuths near the tropopause (100 mbar, 40 km) and taken to be isotropic about the mean wind. These spectra were assumed to propagate vertically through prescribed background winds up into the mesosphere (0.001 mbar, 525 km). In the DSP, the evolution of wave spectra is controlled by background and wave-induced winds. Specifically, this is governed by the monotonically nonincreasing cutoff vertical wave number, m_j, whose variation with height signifies critical level filtering of waves by background wind such that waves with wave numbers higher than m_j break and deposit momentum into the background flow.

$$m_j = \frac{N_{\text{trop}}}{\Phi_1 \sigma_j + \Phi_2 \sigma_T + \Delta V_j} \tag{4}$$

Here N_{trop} is the Brunt-Väisälä frequency at the launch height; σ_j is the root-mean-square speed of the gravity waves travelling in the jth azimuth direction; σ_T is the root-mean-square speed of all the gravity waves; and Φ_1 and Φ_2 are adjustable parameters having values of 1.5 and 0.4, respectively [*Hines*, 1997]. The first term in the denominator represents the Doppler spreading of waves from low to high vertical wave numbers by waves travelling in the jth azimuth, while the second term represents the destabilizing influence of all waves. The final term is the wind shear between the launch height and overlying levels and represents Doppler shifting by the background wind alone. One further parameter is the characteristic horizontal wavelength, which is important for scaling the total wave momentum in the launch spectra. We chose a horizontal wavelength of 200 km, consistent with the wavelength of horizontal structures observed during the Sgr28 stellar occultation [*Sicardy et al.*, 1999].

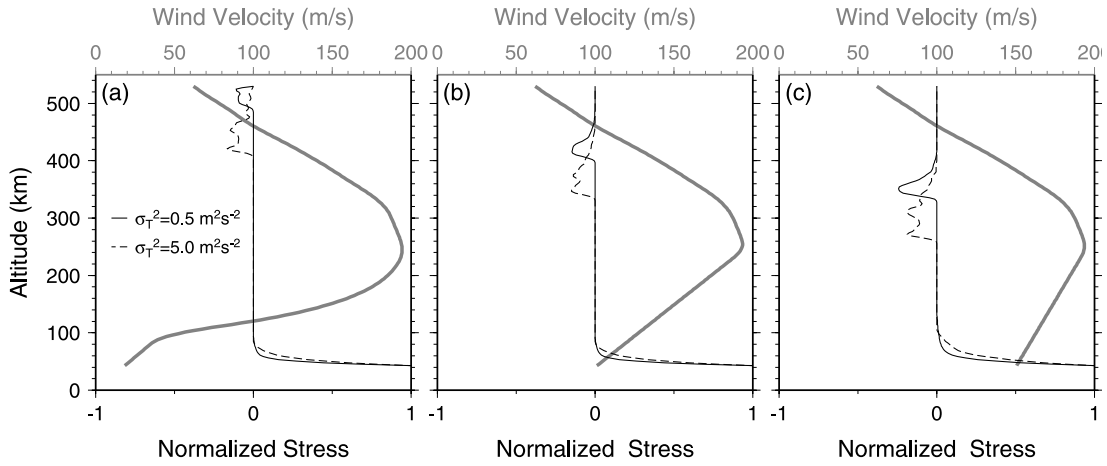

Figure 6. Normalized stress imparted to the zonal flow by breaking gravity waves launched from the tropopause for different wind profiles and gravity wave strengths σ_T^2. Stress is east positive and west negative. Eastward travelling waves break in positive vertical wind shear below the vortex jet, whereas westward propagating waves break in negative wind shear above the vortex jet. Eastward/westward stresses from breaking waves causes an acceleration/drag, which for a steady atmospheric state must be balanced by a residual circulation that transports angular momentum away from/toward the north pole. Faster stratospheric wind speeds and stronger waves cause westward propagating waves to break at lower altitudes.

[47] It is important to note that at present many of the parameters are not well constrained for Titan, so our modeling can only represent the qualitative aspects until further data become available. In our study we have assumed that (1) the variance of the gravity wave wind speed σ_T^2 is similar to values for gravity waves on Earth; (2) the background wind speeds drop linearly (in altitude) from their value at 10 mbar to zero at Titan's surface, in broad agreement with the overall trend from the Huygens results at 15°S [*Bird et al.*, 2005]; and (3) the gravity waves follow a modified Desaubies low wave number spectrum [*Fritts and Alexander*, 2003].

[48] Figure 6 shows the normalized stress exerted on the background flow by gravity wave breaking at 50°N. On earth a gravity wave wind variance σ_T^2 of 1 m^2 s^{-2} is commonly used [*Manzini and McFarlane*, 1998]. On Titan σ_T^2 is not well constrained, so we have used bracketing values of 0.5 and 5.0 m^2 s^{-2}.

[49] The derived temperature profiles contain increased levels of uncertainty in the north polar middle and lower stratosphere. This is caused by trying to observe the coldest region of the stratosphere through the hot stratopause region and results in limited temperature information below about 1 mbar (180 km). Therefore, the derived background thermal wind speeds are not well constrained in this region. Also, the winds derived by *Achterberg et al.* [2008a] assumed a bottom boundary condition of four times solid body rotation speed at 10 mbar based on the Huygens measurements at 15°S. This may not be realistic near the vortex and higher wind speeds may exist in the lower atmosphere. Therefore, in Figure 6 we have used three test wind profiles: thermal wind from *Achterberg et al.* [2008a] with (1) a linear interpolation from 10 mbar to zero at the surface (Figure 6a), (2) wind above the jet core and a linear decrease below the jet core to 100 m s^{-1} at 40 km (Figure 6b), and (3) wind above the jet core and a linear decrease below the jet core to 150 m s^{-1} at 40 km (Figure 6c). At present, it is not possible to constrain winds accurately in Titan's lower atmosphere, so these test wind profiles simply provide a way of determining the sensitivity of gravity wave breaking to plausible background wind fields.

[50] Critical level filtering of eastward propagating waves occurs when the phase speeds of the waves match that of the background flow. Figure 6 shows that this happens almost immediately above the launch altitude due to the large positive vertical wind shear below the vortex jet. This causes waves to break, exerting an eastward stress on the background flow, causing a slight acceleration in the direction of the superrotation, which induces flow away from the pole. Waves travelling westward with respect to the background flow break above the vortex core in a region of negative vertical wind shear. This occurs when the wave amplitude is large enough to cause the local lapse rate to exceed the adiabat, which causes a local instability and precipitates wave breaking. The breaking of these waves exerts a westward stress on the background flow and causes a slight deceleration/drag, which induces a flow toward the pole. Therefore, qualitatively, breaking gravity waves provide a forcing in the right direction to induce a residual circulation near the north pole.

[51] The test cases in Figure 6 show that waves travelling westward with respect to the background flow tend to break when the background winds are similar to those at the launch height. For wind case in Figure 6a, waves tend to break around 500 km, which is too high to provide a residual circulation at the correct altitude to explain the mesospheric depleted zone. However, wind cases in Figure 6b and 6c show that if winds in the lower stratosphere are increased

then the gravity waves break around the right altitude to provide a south-north residual circulation at 350 km, which could result in the observed mesospheric depleted zone. Another possibility is that if vortex winds temporarily fluctuate and weaken, then wave breaking could occur at lower altitudes. More data on the polar winds and gravity wave strength is required before further conclusions can be drawn. At present, we can only say that gravity waves provide a possible mechanism for setting up a residual circulation at Titan's north pole, which could explain the observed mesospheric depleted zone.

[52] Note that the effect of gravity waves on the meridional circulation would be strongest around the north pole, where strong vortex winds filter the gravity wave spectra, leading to wave drag/acceleration above/below the vortex jet. At equatorial latitudes the zonal wind speeds inferred from CIRS [*Achterberg et al.*, 2008a] are reduced compared to the jet core but remain high and could cause the same type of filtering, albeit at a reduced level. However, our measurements of tracer species would not be sensitive to a horizontal residual circulation in equatorial and southern regions as the horizontal composition gradients are too low to result in any measurable enhancements. Therefore, the southern extent of the residual circulation cannot be constrained at present.

[53] The effects discussed in this section have Terrestrial analogues. On Earth, the effects of small-scale gravity waves on the mean meridional circulation are well documented [*Hitchman et al.*, 1989; *Garcia and Boville*, 1994] and are linked with the mesospheric Murgatroyd-Singleton circulation toward the winter pole [*Murgatroyd and Singleton*, 1961]. Our sensitivity study shows that a similar mechanism could also be active in Titan's mesosphere.

[54] Important difference exist between Titan and Earth's stratospheres. In the Earth's winter stratosphere, the effect of gravity waves is small compared to breaking planetary Rossby waves, which act to weaken the polar vortex. Associated with this is a circulation toward the winter pole, the Brewer-Dobson circulation [*Brewer*, 1949; *Dobson*, 1956]. However, on Titan planetary waves are not expected [*Leovy and Pollack*, 1973] so gravity wave effects could become significant. Small-scale gravity wave driving has also been suggested as a mechanism for accelerating Earth's stratospheric polar night jet [*Alexander and Rosenlof*, 1996].

5.4. Gas Tongues and Photochemical Effects

[55] Of the gases studied here, those with the longest lifetimes are C_2H_2 (10 years) and HCN (44 years) [*Wilson and Atreya*, 2004]. The dynamical mixing barrier is most probably not effective over such long timescales so these gases are able to escape the vortex. Mixing to lower latitudes could occur via small-scale wave driving close to the pole and barotropic instabilities equatorward of the vortex jet; both these processes are consistent with Titan's superrotating atmosphere. This equatorward mixing would then produce the observed extended tongues of gas away from the enriched north polar air mass. HCN has a steeper vertical gradient and hence a greater polar enrichment [*Teanby et al.*, 2007; *Vinatier et al.*, 2007] and more pronounced tongue. HCN abundance isolines in this tongue increase in altitude consistently toward the south pole, implying upward advection south of the north polar vortex-dominated region (60°N) due to upwelling in the returning branch of the meridional circulation cell (Figure 4). The upward advection injects HCN-enriched air into the mesosphere, which has the effect of closing off the equatorward flank of the depleted zone and forms a HCN-depleted torus encircling the pole, thus explaining the observed meridional structure.

[56] C_4H_2 also displays a tongue; this is surprising as it has a very short lifetime (2 weeks) and should not be able to survive long enough to escape the vortex and reach equatorial latitudes. This is not an artifact and is visible in four independent profiles covering 0–30°N. Therefore, this observation suggests either a stratospheric source for C_4H_2 at low northern latitudes or a much longer lifetime than expected from photochemical models. The quoted lifetime is most relevant for disc-averaged conditions at 300 km [*Wilson and Atreya*, 2004]. It is possible that the lifetime could be increased significantly in the north because of reduced UV flux and increased shielding by stratospheric haze. However, south of 45°N these effects should not be significant; so the existence of a C_4H_2 tongue there suggests a stratospheric source. We propose that the C_4H_2 tongue is caused by partial polymerization of the C_2H_2 tongue at 200–300 km altitude. Polymerization of C_2H_2 by solar photons to C_4H_2 is thought to occur in Titan's lower atmosphere [*Wilson and Atreya*, 2004] so our results could be the first observational evidence in support of this process and provide a new constraint for photochemical models.

[57] It is interesting to note that C_3H_4 and HC_3N do not show a tongue, even though they have longer lifetimes than C_4H_2. This indicates that net photochemical loss of C_3H_4 and HC_3N is too large to cause observable enrichment at these altitude levels and that photochemical pathways leading to their formation must occur above 500 km.

[58] C_3H_4 and HC_3N have similar photochemical lifetimes (~1 year) [*Wilson and Atreya*, 2004], so should have similar distributions. However, this is not the case, and C_3H_4 enrichment extends about 10–15° of latitude further south than HC_3N, which drops off very rapidly away from the pole. This implies an additional loss process for HC_3N, which is consistent with previous observations of its vertical profile [*Teanby et al.*, 2007; *Vinatier*, 2007] and latitudinal enrichment [*Teanby et al.*, 2008a, 2008b], perhaps incorporation into photochemical hazes [*Wilson and Atreya*, 2003] or photolysis in the lower atmosphere [*Clarke and Ferris*, 1996].

5.5. Meridional Circulation Returning Branch

[59] The distributions of all five tracer species are consistent with a meridional circulation cell that descends below the condensation level (≈100 km), causing subsequent rain out of trace gases onto the north pole. This is consistent with numerical models, which predict a returning branch below 100 km. Condensation prevents homogenization of the atmosphere's composition by removing trace gas enrichment before it can be advected to lower latitudes.

6. Conclusion

[60] Our main result is the much improved definition of the winter polar vortex chemical structure, which is exactly

what is required to understand and model Titan's polar processes. Figure 4 summarizes our overall interpretation of dynamical processes currently occurring in Titan's midwinter stratosphere and mesosphere. Observed composition gradients provide strong evidence for a middle atmosphere mixing barrier around 60°N. This is further corroborated by strong potential vorticity gradients in the same region, suggesting a dynamical origin analogous with Earth's polar vortices. Above the vortex jet a tracer-depleted mesospheric zone encroaches northward up to around 65°N, confining enriched air to high latitudes, whereas in the stratosphere below the vortex jet evidence for transport to lower latitudes is seen. This could be explained by a poleward/equatorward residual circulation above/below the vortex jet, possibly driven by small-scale gravity waves. Enriched gas tongues extending away from the pole suggest horizontal mixing by gravity waves and barotropic instabilities. In addition, our results suggest that polymerization of the C_2H_2 tongue to C_4H_2 occurs at 200–300 km. These features of Titan's atmosphere have been impossible to observe before now and provide new avenues to explore for atmospheric modeling.

[61] **Acknowledgments.** This research was funded by the UK Science and Technology Facilities Council. The authors would like to thank the Cassini-CIRS instrument team, without which this research would not have been possible. We also thank Bryan Lawrence at the British Atmospheric Data Centre for supplying the gravity wave parameterization code.

References

Achterberg, R. K., B. J. Conrath, P. J. Gierasch, F. M. Flasar, and C. A. Nixon (2008a), Titan's middle-atmospheric temperatures and dynamics observed by the Cassini Composite Infrared Spectrometer, *Icarus*, *194*, 263–277.

Achterberg, R. K., B. J. Conrath, P. J. Gierasch, F. M. Flasar, and C. A. Nixon (2008b), Observation of a tilt of Titan's middle-atmospheric superrotation, *Icarus*, *197*, 549–555, doi:10.1016/j.icarus.2008.05.014.

Alexander, M. J., and K. H. Rosenlof (1996), Nonstationary gravity wave forcing of the stratospheric zonal mean wind, *J. Geophys. Res.*, *101*, 23,465–23,474.

Andrews, D. G., J. R. Holton, and C. B. Leovy (1987), *Middle Atmosphere Dynamics*, Academic, Orlando, Fla.

Bézard, B., A. Coustenis, and C. P. McKay (1995), Titan's stratospheric temperature asymmetry—A radiative origin, *Icarus*, *113*, 267–276.

Bird, M. K., et al. (2005), The vertical profile of winds on Titan, *Nature*, *438*, 800–802.

Brewer, A. W. (1949), Evidence for a world circulation provided by the measurements of helium and water vapour distribution in the stratosphere, *Q. J. R. Meteorol. Soc.*, *75*, 351–363.

Clarke, D. W., and J. P. Ferris (1996), Mechanism of cyanoacetylene photochemistry at 185 and 254 nm, *J. Geophys. Res.*, *101*, 7575–7584.

Coustenis, A., et al. (2007), The composition of Titan's stratosphere from Cassini/CIRS mid-infrared spectra, *Icarus*, *189*, 35–62.

Crespin, A., S. Lebonnois, S. Vinatier, B. Bézard, A. Coustenis, N. A. Teanby, R. K. Achterberg, P. Rannou, and F. Hourdin (2008), Diagnostics of Titan's stratospheric dynamics using Cassini/CIRS data and the 2-dimensional IPSL circulation model, *Icarus*, *197*, 556–571, doi:10.1016/j.icarus.2008.05.010.

Dobson, G. M. B. (1956), Origin and distribution of the polyatomic molecules in the atmosphere, *Proc. R. Soc. London, Ser. A*, *236*, 187–193.

Flasar, F. M., et al. (2004), Exploring the Saturn system in the thermal infrared: The Composite Infrared Spectrometer, *Space Sci. Rev.*, *115*, 169–297.

Flasar, F. M., et al. (2005), Titan's atmospheric temperatures, winds, and composition, *Science*, *308*, 975–978.

Friedson, A. J. (1994), Gravity-waves in Titan's atmosphere, *Icarus*, *109*, 40–57.

Fritts, D. C., and M. J. Alexander (2003), Gravity wave dynamics and effects in the middle atmosphere, *Rev. Geophys.*, *41*(1), 1003, doi:10.1029/2001RG000106.

Fulchignoni, M., et al. (2005), In situ measurements of the physical characteristics of Titan's environment, *Nature*, *438*, 785–791.

Garcia, R. R., and B. A. Boville (1994), Downward control of the mean meridional circulation and temperature distribution of the polar winter stratosphere, *J. Atmos. Sci.*, *51*, 2238–2245.

Gierasch, P. J. (1975), Meridional circulation and the maintenance of the Venus atmospheric rotation, *J. Atmos. Sci.*, *32*, 1038–1044.

Hines, C. O. (1997), Doppler-spread parameterization of gravity-wave momentum deposition in the middle atmosphere. Part 2. Broad and quasi monochromatic spectra, and implementation, *J. Atmos. Sol. Terr. Phys.*, *59*, 387–400.

Hinson, D. P., and G. L. Tyler (1983), Internal gravity-waves in Titan's atmosphere observed by Voyager radio occultation, *Icarus*, *54*, 337–352.

Hitchman, M. H., J. C. Gille, C. D. Rodgers, and G. Brasseur (1989), The separated polar winter stratopause—A gravity-wave driven climatological feature, *J. Atmos. Sci.*, *46*, 410–422.

Houghton, J. T. (2002), *The Physics of Atmospheres*, 3rd ed., Cambridge Univ. Press, Cambridge, U.K.

Houghton, J. T., F. W. Taylor, and C. D. Rodgers (1984), *Remote Sounding of Atmospheres*, Cambridge Univ. Press, Cambridge, U.K.

Hourdin, F., O. Talagrand, R. Sadourny, R. Courtin, D. Gautier, and C. McKay (1995), Numerical simulation of the general circulation of the atmosphere of Titan, *Icarus*, *117*, 358–374.

Hourdin, F., S. Lebonnois, D. Luz, and P. Rannou (2004), Titan's stratospheric composition driven by condensation and dynamics, *J. Geophys. Res.*, *109*, E12005, doi:10.1029/2004JE002282.

Hubbard, W. B., et al. (1993), The occultation of 28-Sgr by Titan, *Astron. Astrophys.*, *269*, 541–563.

Irwin, P., N. Teanby, R. de Kok, L. Fletcher, C. Howett, C. Tsang, C. Wilson, S. Calcutt, C. Nixon, and P. Parrish (2008), The NEMESIS planetary atmosphere radiative transfer and retrieval tool, *J. Quant. Spectrosc. Radiat. Transfer*, *109*, 1136–1150.

Jolly, A., Y. Benilan, and A. Fayt (2007), New infrared integrated band intensities for HC_3N and extensive line list for the ν_5 and ν_6 bending modes, *J. Mol. Spectrosc.*, *242*, 46–54.

Kunde, V., et al. (1996), Cassini infrared Fourier spectroscopic investigation, *Proc. Soc. Photo Opt. Instrum. Eng.*, *2803*, 162–177.

Lacis, A. A., and V. Oinas (1991), A description of the correlated k distribution method for modeling nongray gaseous absorption, thermal emission, and multiple-scattering in vertically inhomogeneous atmospheres, *J. Geophys. Res.*, *96*, 9027–9063.

Lait, L. R. (1994), An alternative form for potential vorticity, *J. Atmos. Sci.*, *51*, 1754–1759.

Leovy, C. B., and J. B. Pollack (1973), First look at atmospheric dynamics and temperature variations on Titan, *Icarus*, *19*, 195–201.

Luz, D., F. Hourdin, P. Rannou, and S. Lebonnois (2003), Latitudinal transport by barotropic waves in Titan's stratosphere. II. Results from a coupled dynamics-microphysics-photochemistry GCM, *Icarus*, *166*, 343–358.

Manzini, E., and N. A. McFarlane (1998), The effect of varying the source spectrum of a gravity wave parameterization in a middle atmosphere general circulation model, *J. Geophys. Res.*, *103*, 31,523–31,539.

McIntyre, M. E. (1989), On the Antarctic ozone hole, *J. Atmos. Terr. Phys.*, *51*, 29–33.

McIntyre, M. E., and T. N. Palmer (1983), Breaking planetary-waves in the stratosphere, *Nature*, *305*, 593–600.

Müller-Wodarg, I. C. F., R. V. Yelle, N. Borggren, and J. H. Waite Jr. (2006), Waves and horizontal structures in Titan's thermosphere, *J. Geophys. Res.*, *111*, A12315, doi:10.1029/2006JA011961.

Murgatroyd, R. J., and F. Singleton (1961), Possible meridional circulations in the stratosphere and mesosphere, *Q. J. R. Meteorol. Soc.*, *87*, 125–135.

Niemann, H. B., et al. (2005), The abundances of constituents of Titan's atmosphere from the GCMS instrument on the Huygens probe, *Nature*, *438*, 779–784.

Rannou, P., S. Lebonnois, F. Hourdin, and D. Luz (2005), Titan atmosphere database, *Adv. Space Res.*, *36*, 2194–2198.

Read, P. L., P. J. Gierasch, B. J. Conrath, A. Simon-Miller, T. Fouchet, and Y. H. Yamazaki (2006), Mapping potential-vorticity dynamics on Jupiter. I: Zonal-mean circulation from Cassini and Voyager 1 data, *Q. J. R. Meteorol. Soc.*, *132*, 1577–1603.

Richardson, M. I., A. D. Toigo, and C. E. Newman (2007), PlanetWRF: A general purpose, local to global numerical model for planetary atmospheric and climate dynamics, *J. Geophys. Res.*, *112*, E09001, doi:10.1029/2006JE002825.

Rodgers, C. D. (1976), Retrieval of atmospheric temperature and composition from remote measurements of thermal radiation, *Rev. Geophys. Space Phys.*, *14*(4), 609–624.

Rossow, W. B., and G. P. Williams (1979), Large-scale motion in the Venus stratosphere, *J. Atmos. Sci.*, *36*, 377–389.

Schoeberl, M. R., and D. L. Hartmann (1991), The dynamics of the stratospheric polar vortex and its relation to springtime ozone depletions, *Science*, *251*, 46–52.

Sicardy, B., et al. (1999), The structure of Titan's stratosphere from the 28 Sgr occultation, *Icarus*, *142*, 357–390.

Strobel, D. F. (2006), Gravitational tidal waves in Titan's upper atmosphere, *Icarus*, *182*, 251–258.

Teanby, N. A. (2007), Constrained smoothing of noisy data using splines in tension, *Math. Geol.*, *39*, 419–434.

Teanby, N. A., and P. G. J. Irwin (2007), Quantifying the effect of finite field-of-view size on radiative transfer calculations of Titan's limb spectra measured by Cassini-CIRS, *Astrophys. Space Sci.*, *310*, 293–305.

Teanby, N. A., et al. (2006), Latitudinal variations of HCN, HC_3N, and C_2N_2 in Titan's stratosphere derived from Cassini CIRS data, *Icarus*, *181*, 243–255.

Teanby, N. A., et al. (2007), Vertical profiles of HCN, HC_3N, and C_2H_2 in Titan's atmosphere derived from Cassini/CIRS data, *Icarus*, *186*, 364–384.

Teanby, N. A., P. G. J. Irwin, R. de Kok, and C. A. Nixon (2008a), Dynamical implications of seasonal and spatial variations in Titan's stratospheric composition, *Philos. Trans. R. Soc. London, Ser. A*, in press.

Teanby, N. A., et al. (2008b), Global and temporal variations in hydrocarbons and nitriles in Titan's stratosphere for northern winter observed by Cassini/CIRS, *Icarus*, *193*, 595–611.

Tokano, T., F. M. Neubauer, M. Laube, and C. P. McKay (1999), Seasonal variation of Titan's atmospheric structure simulated by a general circulation model, *Planet. Space Sci.*, *47*, 493–520.

Vinatier, S. (2007), Analyse des spectres infrarouges thermiques émis par l'atmosphère de Titan enregistrés par l'instrument Cassini/CIRS, Ph.D. thesis, Univ. Denis Diderot Paris VII, Paris.

Vinatier, S., et al. (2007), Vertical abundance profiles of hydrocarbons in Titan's atmosphere at 15°S and 80°N retrieved from Cassini/CIRS spectra, *Icarus*, *188*, 120–138.

Walterscheid, R. L., and G. Schubert (2006), A tidal explanation for the Titan haze layers, *Icarus*, *183*, 471–478.

Wilson, E. H., and S. K. Atreya (2003), Chemical sources of haze formation in Titan's atmosphere, *Planet. Space Sci.*, *51*, 1017–1033.

Wilson, E. H., and S. K. Atreya (2004), Current state of modeling the photochemistry of Titan's mutually dependent atmosphere and ionosphere, *J. Geophys. Res.*, *109*, E06002, doi:10.1029/2003JE002181.

R. K. Achterberg and C. A. Nixon, Department of Astronomy, University of Maryland, College Park, MD 20742, USA.

B. Bézard and S. Vinatier, Observatoire de Paris, LESIA, Meudon, F-92195 France.

S. B. Calcutt, R. de Kok, P. G. J. Irwin, S. Osprey, P. L. Read, and N. A. Teanby, Atmospheric, Oceanic and Planetary Physics, University of Oxford, Oxford OX1 3PU, UK. (teanby@atm.ox.ac.uk)

B. J. Conrath and P. J. Gierasch, Department of Astronomy, Cornell University, Ithaca, NY 14853, USA.

F. M. Flasar, NASA Goddard Space Flight Center, Code 693, Greenbelt, MD 20771, USA.